CILAMCE 2017

Florianópolis - Santa Catarina - Brazil

CONVECTION-CONDUCTION MODEL FOR A TROMBE WALL CONFIGURATION

Taynara Geysa Silva do Lago
Kamal Abdel Radi Ismail
taynaragsl@fem.unicamp.br
kamal@fem.unicamp.br
State University of Campinas - UNICAMP
Faculty of Mechanical Engineering, Department of Energy, 13083-860, Campinas, São Paulo, Brazil

Abstract.*The present study handles the conjugate heat transfer problem in a square cavity heated on one wall and cooled at the other parallel wall having an internal conducting solid body. The model is based on the equations of mass conservation, momentum and the energy equations. The discretization of the equations is realized by using the finite volume method in conjunction with the power-law scheme. Flow and temperature fields are produced and the results are presented in terms of temperature and velocity distributions in various parts of the system. The Nusselt number and the system thermal performance as a function of the Rayleigh number are also evaluated and presented.*

Keywords: *Natural convection, Cavity, Trombe wall, Passive comfort, Thermal wall*

1 INTRODUCTION

Natural convection in cavities is one of the classic problems of heat transfer having an extensive number of numerical and experimental approaches since the second half of the 20th century. The most common way to study the phenomenon of natural convection in cavities is that where a rectangular cavity is heated and cooled by the side walls or the lower and upper walls, respectively, while the remaining walls are considered as adiabatic. In the laterally heated cavity, the perpendicular configuration imposed between the gravity vector and the temperature gradient causes the fluid movement to occur, with no possibility of equilibrium between the thrust and viscous forces. Other cavity configurations are also found in the literature, which are usually square or rectangular, combining fully or partially heated / cooled walls under constant temperature or heat flow.

Trombe wall system consists of a massive wall installed at a small distance from a glazing. The wall absorbs solar radiation and transmits part of it into the dwelling by natural convection through the solar chimney formed by the glazing on one side and the wall on the other. The air circulates through the vents at the bottom and top of the wall into the adjacent room. The natural convection is then controlled by these vents. The various parameters are: Rayleigh number (from 10^3 to 10^6), dimensionless conductivity of bounding wall (from 0 to 100), dimensionless wall thickness (from 0 to 0.6) and dimensionless wall length (0.5 to 1).

A review of the literature indicates that previous analyses are related to two major categories with various boundary conditions: (1) those treating the natural convection in cavities with internal solid; (2) those treating the heat transfer in the entire system including the Trombe wall collector and the adjacent room.

In the first category, the investigations were typically performed using a body of several size where the body itself might be heat-generating, adiabatic, or conductive. House et al. (1990) analyzed the effect of the size and thermal conductivity of a single solid body positioned in the center of an enclosure heated and cooled from its sides. The heat transfer in the enclosure is governed by Rayleigh and Prandtl numbers, the size of the body and its thermal conductivity.

Mezrhab et al. (2005) described a numerical study of the radiation-natural convection interactions in a differentially heated cavity with an inner body. A specifically developed numerical model, based on the finite-volume method, is used for the solutions of the governing differential equations. The SIMPLER algorithm for the pressure–velocity coupling is adopted. The fluid (air) is considered transparent to the radiation. The surface emissivity, the Rayleigh number, and the thermal conductivity ratio were varied parametrically. For Pr = 0.71 and relatively wide ranges of the other parameters, results are reported in terms of isotherms, streamlines, average Nusselt-numbers across the enclosure, local Nusselt-numbers at the hot and cold walls, vertical and horizontal median velocities and horizontal walls, temperature distributions.

Ha et al. (1999) realized a numerical study to investigate transient heat transfer and flow phenomena of natural convection of three different fluids of sodium, air, and water in a vertical square enclosure within which a centered, squared, heat-conducting body generates heat. The analysis proceeds by observing variations of the streamlines and isotherms with respect to the dimensionless time for different Rayleigh numbers, temperature-difference ratios, Prandtl numbers, and thermal conductivity ratios. The variations of average Nusselt numbers on the hot and cold walls are also presented with respect to the dimensionless time, to show the transient behavior of overall heat transfer characteristics inside the enclosure.

Ha et al. (2002) and Ha et al. (2002) studied the effect of an adiabatic body in an enclosure heated from the bottom and cooled from the top. The authors showed that there is a range of Rayleigh number for which the Nusselt number achieves a steady behavior after few oscillations. This steady behavior becomes periodic oscillatory as the Rayleigh number increases.

In the second category, Yedder and Bilgen (1991) studied thermal performance of classical Trombe wall solar collector system. They assumed that the flow is laminar and two-dimensional, the glazing is isothermal and the solar heat absorbed by the wall is transferred to the air in the channel with a constant flux by natural convection and to the adjacent room by conduction and then by convection. They used square cavity, rectangular cavity with aspect ratios of 5. The Nusselt number and the system thermal performance as a function of the Rayleigh number were also presented and discussed.

Kundakci and Yilmaz (2012)compared a simulation model with experimental results of a Trombe wall façade of a model test in Izmir, Turkey for two days. They found that the simulation model tends to overpredict the outlet air temperature in the channel when the solar radiation is weak. Liu et al. (2013) investigated the storage behavior of the Trombe wall by experimental and numerical prediction Rabani et al. (2015) studied a new designed Trombe wall for Yadz, Iran in winter. From the comparison of numerical and experimental results, the authors concluded that the new design Trombe wall is able to keep the room warm.

Hernandez et al. (2016) investigated an R-TW (room with a Trombe wall)system. The climatic data of the colder and warmer days of 2014 were used to evaluate the behavior of R-TW in two cities of Mexico with cold weather (Huitzilac and Toluca). The simulations were done with an internal code based on the Finite Volume Method. It has been found that the losses of thermal energy through the semitransparent wall are about 60% of the solar radiation incident on the system. Despite thermal losses, the system gets enough energy to keep the air inside the room with a temperature above 35°C. For both cities during the coldest day, the maximum stored energy is about 109 MJ during the day. The hottest is about 70 MJ. This energy is supplied from the storage wall to the air inside the room during periods without sunshine.

In this work, a square cavity heated and cooled by the sidewalls with an inserted rectangular solid. The dimensions of the system are: solid with variation of the height and thickness, the cavity with ratio of H/L=1 in width and height and a distance of about 0.1m from the solid in Relation to the west wall. The conductivity of the solid is characterized by the ratio of the conductivities of the solid to the fluid. The paper presents the mathematical model of the problem and the validation of the computational program considering the temperature conditions. The results from the numerical solution are presented and discussed.

2 MATHEMATIC OF MODEL

The problem studied has as domain a two-dimensional cavity of length L, height H, with aspect ratio H / L = 1, filled with fluid of thermal conductivity k_f and a rectangular solid block of varying thickness and length positioned inside. The upper and lower boundaries of the domain are adiabatic while the left border is defined as constant high temperature, and the right border is defined as constant low temperature. In the interior of the cavity the block will be considered conductor of thermal conductivity k_s. The domain of the problem and the definitions of the boundary conditions used in the work are shown in Fig. 1.

The model is based on the conservation equations of mass, energy and momentum in its two-dimensional and permanent forms. It is assumed that the flow is laminar and incompressible, so the fluid density is considered constant, except for the buoyancy term for which the Boussinesq approximation applies. Field forces acting on the mass of fluid as a whole are admitted as due only to the force of gravity acting in the vertical and downward direction. In the energy equation it is considered that the viscous dissipation and the compression work are negligible. All the thermo-physical properties will be considered constant, except for the density in the buoyancy term.

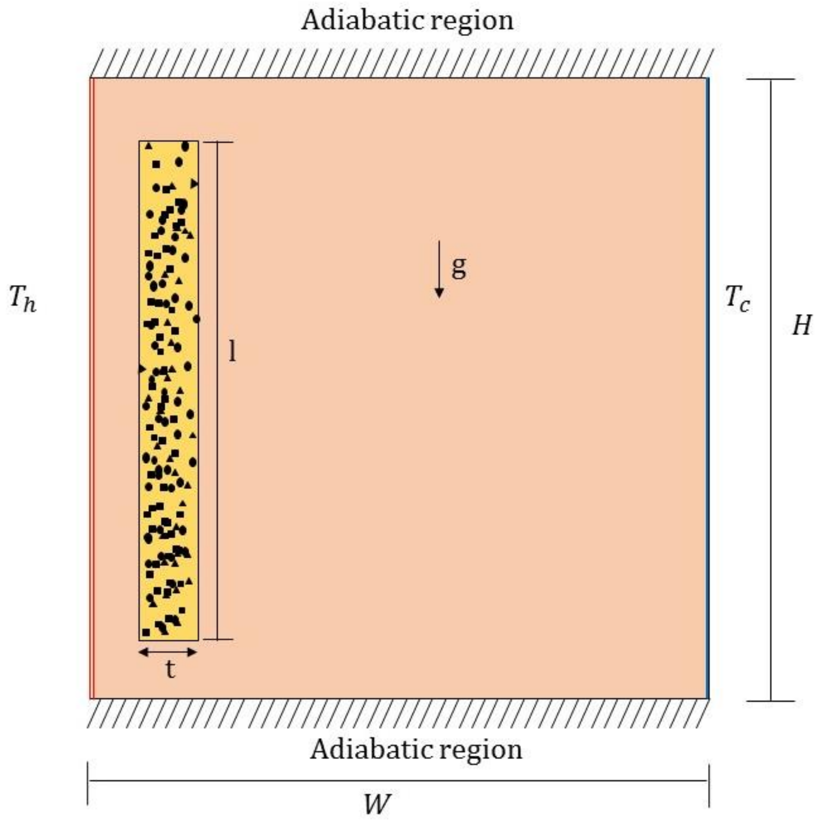

Figure 1. Scheme of probem domain

2.1 Conservation equations for the fluid

The conservation equations for the study of natural convection in the fluid field, in closed cavities have the following hypotheses:

a) Permanent regime;

b) Two-dimensional and laminar flow;

c) Incompressible flow;

d) Function neglected viscous dissipation;

e) Physical properties of the fluid (ρ_f, μ, c_{pf}, k_f) constants, except the specific mass in terms of buoyancy;

f) No internal heat generation.

Through the above hypotheses the conservation equations in dimensional form for the fluid domain are,

Continuity,

$$\frac{\partial u}{\partial x} + \frac{\partial v}{\partial y} = 0. \tag{1}$$

Momentum,

$$u\frac{\partial u}{\partial x}+v\frac{\partial v}{\partial y}=-\frac{1}{\rho_f}\frac{\partial p}{\partial x}+\nu\left(\frac{\partial^2 u}{\partial x^2}+\frac{\partial^2 u}{\partial y^2}\right). \tag{2}$$

$$u\frac{\partial u}{\partial x}+v\frac{\partial v}{\partial y}=-\frac{1}{\rho_f}\frac{\partial p}{\partial y}+\nu\left(\frac{\partial^2 v}{\partial x^2}+\frac{\partial^2 v}{\partial y^2}\right)+g\beta(T-T_C). \tag{3}$$

And Energy,

$$u\frac{\partial T}{\partial x}+v\frac{\partial T}{\partial y}=\frac{K_f}{\rho_f cp_f}\left(\frac{\partial^2 T}{\partial x^2}+\frac{\partial^2 T}{\partial y^2}\right). \tag{4}$$

2.2 Conservation equations for solid

The velocity components u and v are zero in the solid domain. The equation of Energy in the dimensional form for the solid domain, presents the following hypotheses:

a) Permanent regime;

b) Physical properties of the solid (k_s, ρ_s, c_{ps},) are constant;

c) Without internal heat generation.

Through the above considerations, the conservation equation of energy in the form dimensional for the solid domain, is:

$$\frac{K_s}{\rho_s cp_s}\left(\frac{\partial^2 T}{\partial x^2}+\frac{\partial^2 T}{\partial y^2}\right)=0. \tag{5}$$

2.3 Non-dimensional equations

In order to generalize the numerical solution of the problem the following dimensionless variables are introduced for the fluid and solid domains:

$$X=\frac{x}{L},\ Y=\frac{y}{L}. \tag{6}$$

$$U=\frac{uL}{\nu},\ V=\frac{vL}{\nu}. \tag{7}$$

$$P=\frac{p+\rho gy}{\rho\left(\frac{\nu}{L}\right)^2}. \tag{8}$$

$$\theta=\frac{T-T_c}{T_h-T_c}. \tag{9}$$

$$Ra = \frac{g\beta(T_h - T_c)L^4}{\nu\alpha}. \tag{10}$$

$$Pr = \frac{\nu}{\alpha}. \tag{11}$$

Substituting the dimensionless variables into the equations of the fluid and solid regions and following the book of Patankar (1980) for conjugate problems of convection and conduction, one can rewrite the governing equations of the problem in its dimensionless form as follows:

$$\frac{\partial U}{\partial X} + \frac{\partial V}{\partial Y} = 0. \tag{12}$$

$$U\frac{\partial U}{\partial X} + V\frac{\partial V}{\partial Y} = -\frac{\partial P}{\partial x} + \Gamma\left(\frac{\partial^2 U}{\partial X^2} + \frac{\partial^2 U}{\partial Y^2}\right). \tag{13}$$

$$U\frac{\partial U}{\partial X} + V\frac{\partial V}{\partial Y} = -\frac{\partial P}{\partial y} + \Gamma\left(\frac{\partial^2 V}{\partial X^2} + \frac{\partial^2 V}{\partial Y^2}\right) + \frac{Ra}{Pr}\theta. \tag{14}$$

$$U\frac{\partial \theta}{\partial X} + V\frac{\partial \theta}{\partial Y} = \frac{K}{Pr}\left(\frac{\partial^2 \theta}{\partial X^2} + \frac{\partial^2 \theta}{\partial Y^2}\right). \tag{15}$$

Where Γ is a general diffusion coefficient which is equal to 1 for fluid region and 10^{20} for the region of the solid, and K is a thermal conductivity ratio that is equal to 1 in the region of fluid e $k^* = k_s / k_f$, in solid region.

2.4 The boundary conditions

In the region of the solid U = V = 0. Equations (11) to (14) are subjected to the contour conditions presented below in their dimensionless form for cavity:

$X = 0 \rightarrow U = V = 0, \theta = 0$

$X = 1 \rightarrow U = V = 0, \theta = 1$

$Y = 0 \rightarrow U = V = 0, \quad \partial\theta/\partial Y = 0$

$Y = 1 \rightarrow U = V = 0, \quad \partial\theta/\partial Y = 0$

2.5 Nusselt Number

The convective heat exchange is characterized by the mean Nusselt number in the cavity. The Local Nusselt number for surfaces is:

$$Nu_L = \frac{1}{2}\left.\frac{\partial \theta}{\partial X}\right|_S. \tag{16}$$

where S can be the left or right surface.

The average Nusselt number for surfaces is:

$$Nu = \frac{1}{S}\int_{s} Nu_{L}\big|_{s} dS. \tag{17}$$

3 NUMERICAL PROCEDURE

After establishing the equations that represent the mathematical model and the boundary conditions, the next step is to solve the problem. It is verified that due to the complexity of the equations and boundary conditions, an analytical solution is not feasible and therefore should thus use numerical resolution techniques. Then, the solution of the dimensionless equations is obtained numerically using the Finite Volume Method in conjunction with the Power-law scheme for discretizing the convective and diffusive energy fluxes. The computational code, written in FORTRAN language, uses SIMPLE algorithm for coupling of pressure and velocity, which is based on a process of velocity field correction based on a pressure field that allows satisfying the mass conservation equation, and the TDMA method in the solution of the systems of equations.

It is convenient to express the conservation equations in their generic form with respect to the conservation of a property φ. For the two-dimensional case in permanent regime, this equation can be written in its conservative form with constant Γφ according to the equation below:

$$\frac{\partial}{\partial x}(\rho u \phi) + \frac{\partial}{\partial x}(\rho v \phi) = \Gamma_{\phi}\left(\frac{\partial^2 \theta}{\partial x^2} + \frac{\partial^2 \theta}{\partial y^2}\right) + S. \tag{18}$$

Where the terms on the left side of the equation correspond to the advective transport of property φ and the first two terms on the right side correspond to the diffusive transport of this property, where Γ_{φ} is the diffusive transport coefficient, and the last term of the equation represents a source term. Equation (18) is used to represent the conservation equations from the assignment of specific values for the variables φ, Γ, ρ and S. The representation of the dimensionless equations, for example, is done by assigning the values shown in Table 1 to the variables of Eq. (18) for each conservation equation indicated in the table.

Table 1. Values of φ, Γ, ρ and S for conservation equations

Conservation Principles	ϕ	ρ	Γ	S
Mass	1	1	0	0
Momentum - X	U	1	Flui. = 1 Sol.=10^{20}	$-\frac{\partial P}{\partial X}$
Momentum - Y	V	1	Flui. = 1 Sol.=10^{20}	$-\frac{\partial P}{\partial Y}+\frac{Ra}{Pr}\theta$
Energy	θ	1	$\frac{K}{Pr}$	0

The domain was divided into a uniform grid in a way that the solid-fluid interface and the domain boundaries coincide with the faces of the control volume. The harmonic mean was used to determine the diffusive coefficients at the interfaces of the control volume (Patankar, 1980). The component velocities were allocated in a staggered grid.

Equations (12)-(15) are solved for the entire domain. In the solid region, the coefficient of the diffusion terms of Eqs. (13) and (14) is set to a high number of 10^{20} such that the velocity gets close to zero. The process of iterative solution starts from an arbitrary f field and the convergence criterion is reached when Eq. (19) is satisfied.

$$\sum_{i,j}\left|\frac{\phi_{ij}^{n}-\phi_{ij}^{n+1}}{\phi_{ij}^{n}}\right|\leq\varepsilon\,. \tag{19}$$

where ϕ represents the variables U, V, T and P. The variable n is the iteration order and the value of ε chosen is 10^5.

It was made several numerical tests with the purpose of optimizing the code computational, for establish the size of the mesh that does not influence the results and determine the conditions of stability and numerical convergence.

A mesh study was performed for the critical case of Ra = 10^6 and k*=100 with 48x48, 88x88 and 148x148 volumes, with mesh refinement close to solid surfaces. The Nusselt number variation was 0.15% with volumes increasing from 88x88 to 148x148. In this way, the results of the work were obtained for a mesh of 88x88 volumes.

The validation of the problem was performed by comparing the Nusselt number with literature results for cavities with or without the internal solid, showing good agreement. The results for the dimension of solid of the present problem are not available in the literature.

The average Nusselt number is compared with that given by Davis (1983), Frederick (1989) and Palanigounder et al. (2008) for the different values of the Rayleigh number as shown in Fig. 2 and Table 2. In the Fig. 3, it is clear that the present solution of streamlines is very close to Davis result. These results provide confirmation of the accuracy of the present numerical method to study the natural convection in a cavity with partially thermally active side walls.

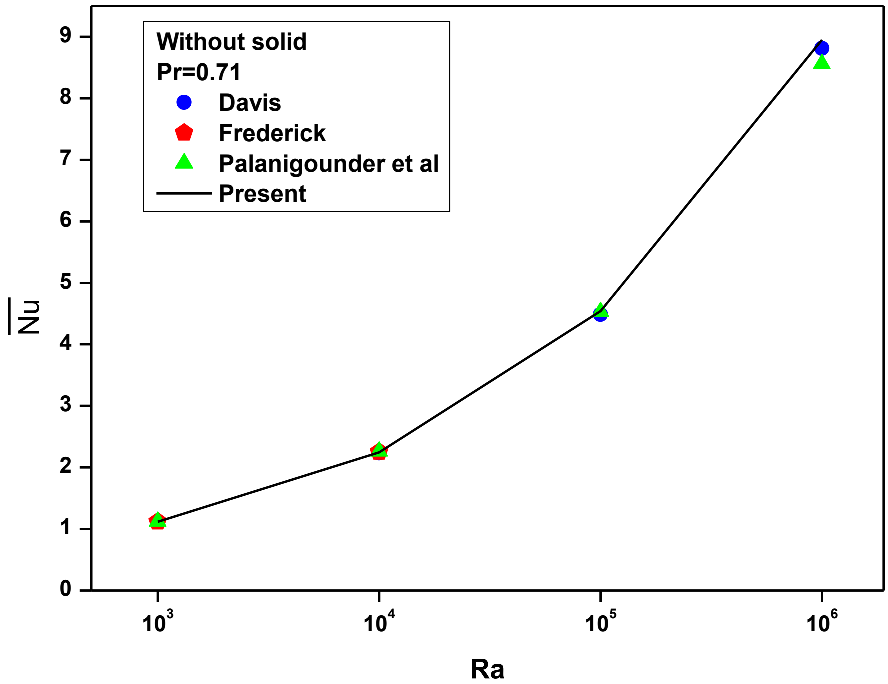

Figure 2. Average Nusselt number vs Rayleigh number for Pr = 0.71

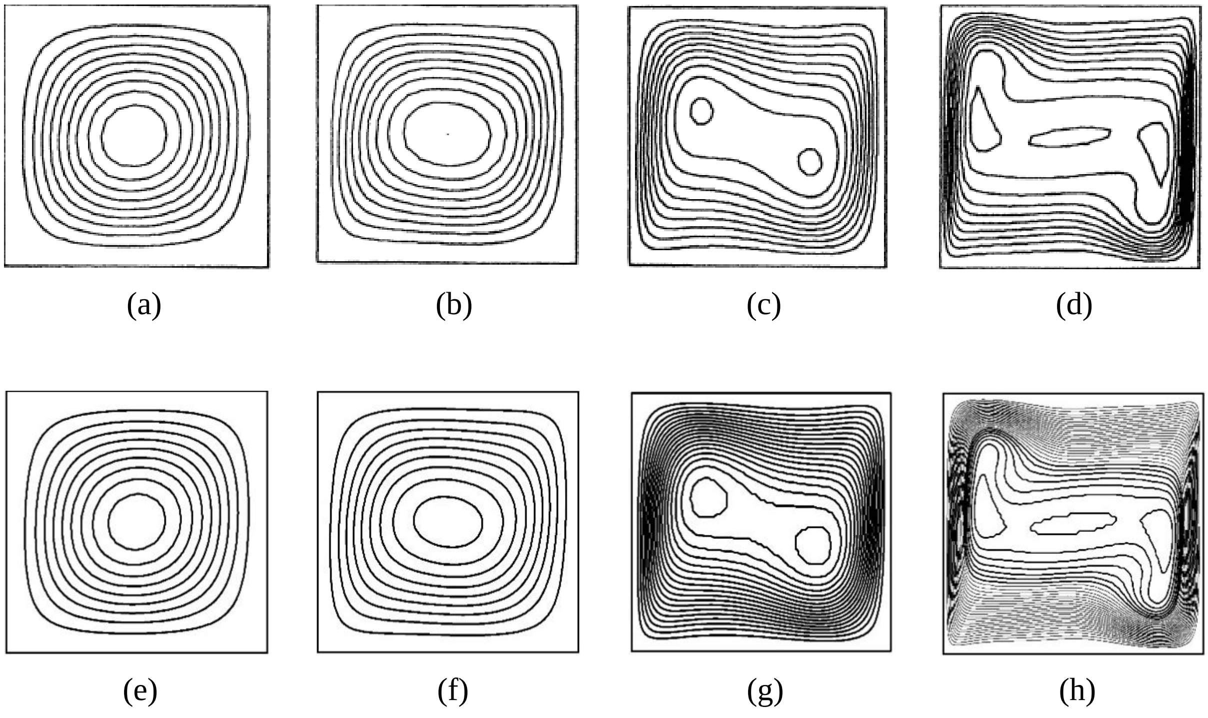

Figure 3. Comparison of the streamlines of the cavity without a body. (a)-(d) Davis results for 10^3(contours at -1.174), 10^4(contours at -5.071), 10^5(contours at -9.507), 10^6(contours at -16.27). (e)-(h) Presents results for 10^3(contours at -1.527), 10^4(contours at -6.727), 10^5(contours at -12.545), 10^6(contours at -22.290)

Table 2. Comparison of average Nusselt numbers for different Rayleigh numbers, with Pr=0.71

	Nu			
Ra	Davis	Frederick	Palanigounder et al.	Present
10^3	1.116	1.11869	1.12059	1.1174
10^4	2.234	2.24999	2.26175	2.2478
10^5	4.487	-	4.53004	4.5420
10^6	8.811	-	8.55873	8.9509

On the other hand, in order to validate the code for cavity with solid, the results were generated and compared with results available in the literature on cavity heated and cooled from the side with an internal conducting solid of known size (Table 3). Table 3 shows the average Nusselt number for a grid of 88x88 control volumes with Pr=0.71. The size of the solid chosen for comparison in the literature occupies the entire central region of the cavity. As can be seen good agreement is obtained indicating that the numerical code predicts satisfactory results for the conjugate heat transfer problem.

Table 3. Comparison of average Nusselt numbers for different Rayleigh numbers

	$Ra=10^5$, t/L=0.5 and w/H=0.5	
	k*=0.2	k*=5
Present	4.644	4.337
House et al. (1990)	4.624	4.324
Zhao et al. (2007)	4.660	4.362
Bhave et al. (2006)	4.645	4.338
Lima and Ganzarolli (2016)	4.63	4.32

4 RESULTS AND DISCUSSION

The geometrical parameters chosen based for the Trombe wall system: A= H/L=1.0; B=s/L=1/33; C=t/L=0.07 to 0.6; D=w/H=0.5, to 1. The thermophysical parameters are $Ra=10^3$ to 10^6 and $k^* = k_s/k_f$ = 1(corresponding to isolant wall) to 100 (corresponding to stone wall). Various simulations were carried out for the range of geometrical and thermophysical parameters discussed.

4.1 Temperature and velocity fields

In the cavity, the fluid is cooled at the cold wall and the temperature gradient formed is normal to the acceleration vector of gravity. This configuration between the temperature gradient and the gravity vector near the cooled wall generates the downward movement of the fluid. This movement remains until the fluid mass encounters the hot wall where it is heated and decelerated, changing direction.

The temperature fields shown in Fig. 4 indicate the tendency for thermal layer formation limit at the cooled and heated walls with increasing Rayleigh number. For Ra = 10^3, the temperature field approaches the pure conduction mechanism, with the isotherms presenting a near form of diagonal symmetry. As the Rayleigh number increases, the circulation of fluid in the core of the cavity tends to uniformize its temperatures forming a region of approximately homogeneous temperature which takes up almost the entire lower half of the cavity. This process leads to a reduction in the temperature difference between the vertical walls along the vertical axis of the cavity.

The isotherms for the cavity with a conducting body with C = 0.07 e D=0.7 are shown in Fig. 4 for Ra= 10^3and10^6. The isotherms for the cavity without such a body are also show as a reference in Fig. 4(a), (e), (i) and (m). For small solids, the solid area is small relative to the area filled with fluid. The pattern of isotherms of the enclosure with an internal body differs little from that of the enclosure without a body. In Fig. 4, the solid with the same thermal conductivity of the fluid (k*=1) shows in the region of the solid an isotherm pattern similar to that of the same region of the enclosure without the body and the same Rayleigh number. Even for a high-heat conducting body (k*=20 and k*=100), heat transfer through the solid results only in small distortions of the isotherms in the region near the solid. As the Rayleigh number increases the influence of the body on the isotherms pattern diminishes when compared with the solid without the body. It can be seen that increasing the number of Rayleigh causes the maximum temperature of the fluid in the cavity to be reduced and that the region where the fluid reaches its maximum temperature is pressed against the vertical adiabatic wall of the cavity. This is due to the increase in velocity of the fluid flowing near the heated wall due to the increase in Rayleigh number.

In Fig. 4, the insertion of the solid with C = 0.07 and D = 0.7 shows little influence on the cavity temperature fields as compared to the no-cavity for all Rayleigh numbers studied. As the size of the block increases with C = 0.11 and D = 0.9 (Fig. 5), it is important to note that for Ra = 10^6 the changes in the temperature fields begin to be observed for larger blocks when compared to the smaller Rayleigh numbers, That is, the larger the Rayleigh number, larger blocks can be inserted into the cavity without changing the cavity temperature field.

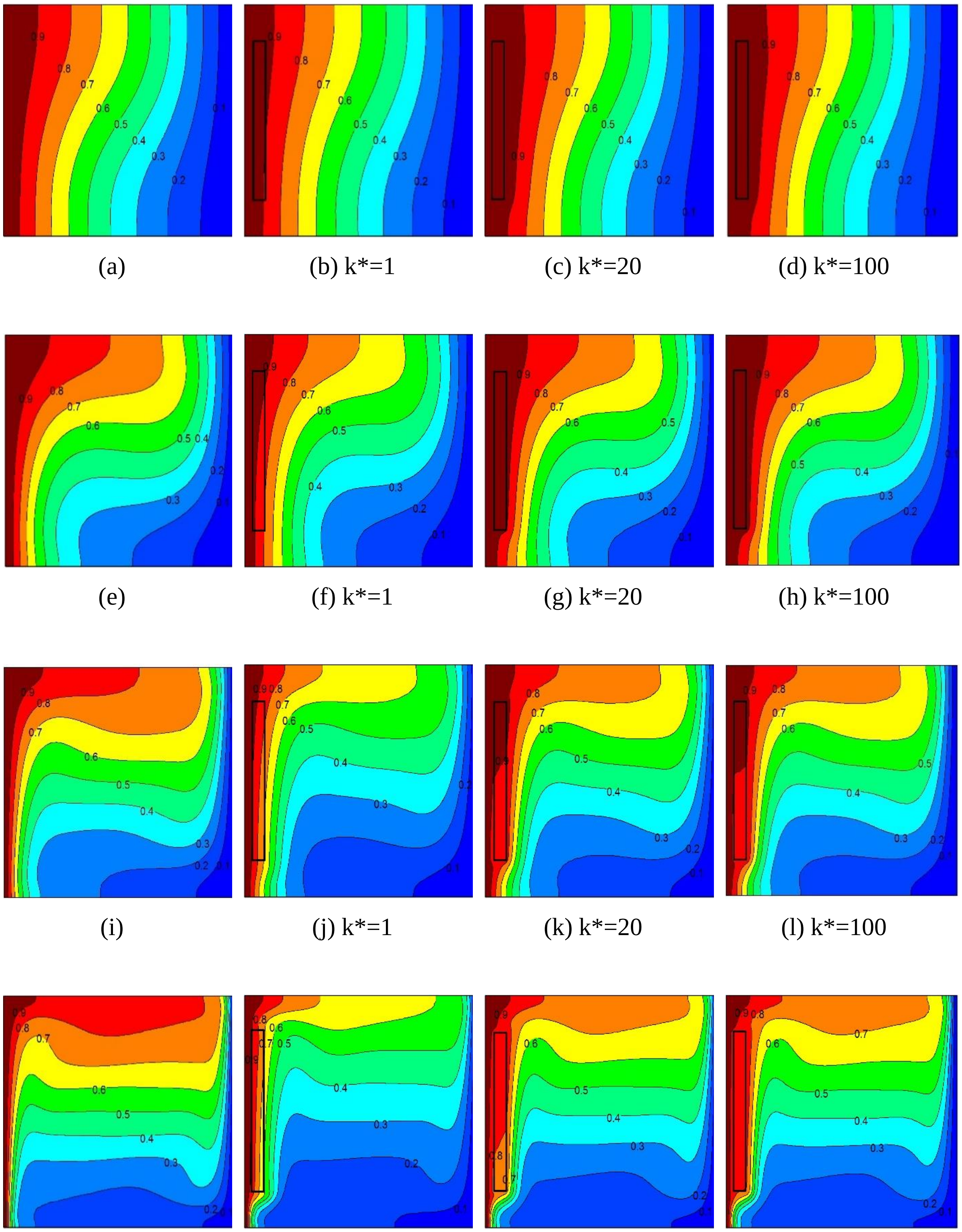

(a) (b) k*=1 (c) k*=20 (d) k*=100

(e) (f) k*=1 (g) k*=20 (h) k*=100

(i) (j) k*=1 (k) k*=20 (l) k*=100

(m) (n) k*=1 (o) k*=20 (p) k*=100

Figure 4. Isotherms for the cavity with C=0.07, D=0.7 and without a body with (a) e (d) Ra $=10^3$, (e) e (h) Ra $=10^4$, (i) e (l) Ra $=10^5$ and (m) e (p) Ra $= 10^6$

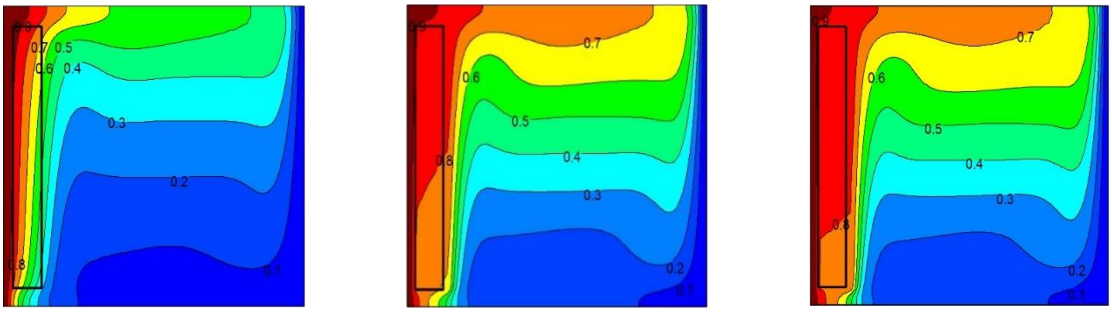

(a) k*=1 (b) k*=20 (c) k*=100

Figure 5. Isotherms for the cavity with C=0.11 and D=0.9 with Ra=10^6

The cavity has flow in a single cell rotating clockwise (Fig. 6). The shapes of the streamlines in the cavity suggest the formation of jets on the walls where the temperature is constant. As the number of Rayleigh and consequently the convective flow increases, the stream lines become denser near the walls of the cavity.

The higher velocity zones U and V move from a region approximately in the middle of the heated and cooled walls towards the upper left corner and the lower right corner of the cavity, characterized by the narrowing of the stream lines. The flow in the cavity without block forms a vortex that rotates clockwise.

The streamlines are shown in Fig. 6 for a cavity with a long rectangular solid: air is heated in the solid wall, it circulates at the top, and cools down, it circulates again in the bottom of the cavity and below the solid block. As expected, the circulation is stronger as Ra increases, causing narrowing of stream lines and vortices.

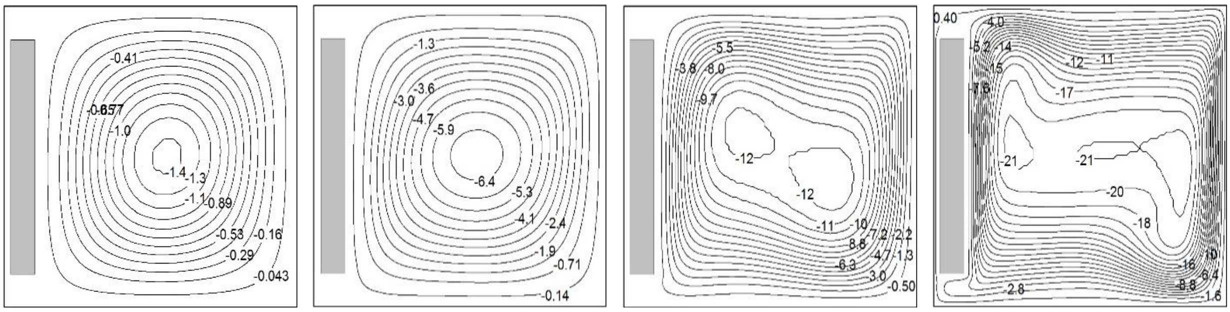

(a) (b) (c) (d)

Figure. 6. Streamlines of the cavity with B=0.09, D=0.8 for k*=20 and solid with (a) e (d) Ra =10^3, 10^4, 10^5, 10^6

The profile of the component V shows higher velocity values in the region of the upward flow near the heated wall followed by a region of near uniform velocity, descending and of smaller magnitude, which extends over the remainder of the profile. The U component presents higher velocities in the peripheral regions of the profile and of smaller magnitude in the central region of the cavity.

For Ra = 10^5 and 10^6, the central vortex is pressed between the walls of the cavity and the block generating new rotating cells in the channel and the maximum stream function points of the cavity are shifted towards the formed vortices. The vortices formed when Ra = 10^5 and 10^6 by the isolines of the stream function are located in the central part.

4.2 Heat transfer

Heat transfer as a function of various parameters is evaluated and presented as average Nusselt number, Eq. (11), in terms of dimensionless parameters in Figs. 8 and 9. Average Nusselt number as a function of the Rayleigh number with C and k* as parameters is shown in Fig. 9. Heat transfer increases with increasing Rayleigh number, decreasing wall thickness and increasing wall conductivity. As observed earlier in Fig. 8, it is seen that for Ra =10^3 the heat transfer is dominated by conduction. For increasing k* and C, convection becomes equally important at Ra >10^4. As Ra increases, the convection heat transfer becomes the dominant heat transfer mode.

The effect of wall conductivity on the heat transfer is shown in Fig. 9. It is seen that Nusselt an increasing function of k*, weak at low Ra and strong at high Ra with the same trend for different wall thicknesses. This is due to the fact that convection is not affected beyond a wall conductivity above which the wall inner surface temperature becomes almost the same as that of the wall outer surface. In fact, for k*≥ 5, there is only a small temperature gradient in the massive wall. It should be noted that the dimensionless conductivities for various construction materials are usually between 1 and 10, well insulated partitions and walls having k*≈1.

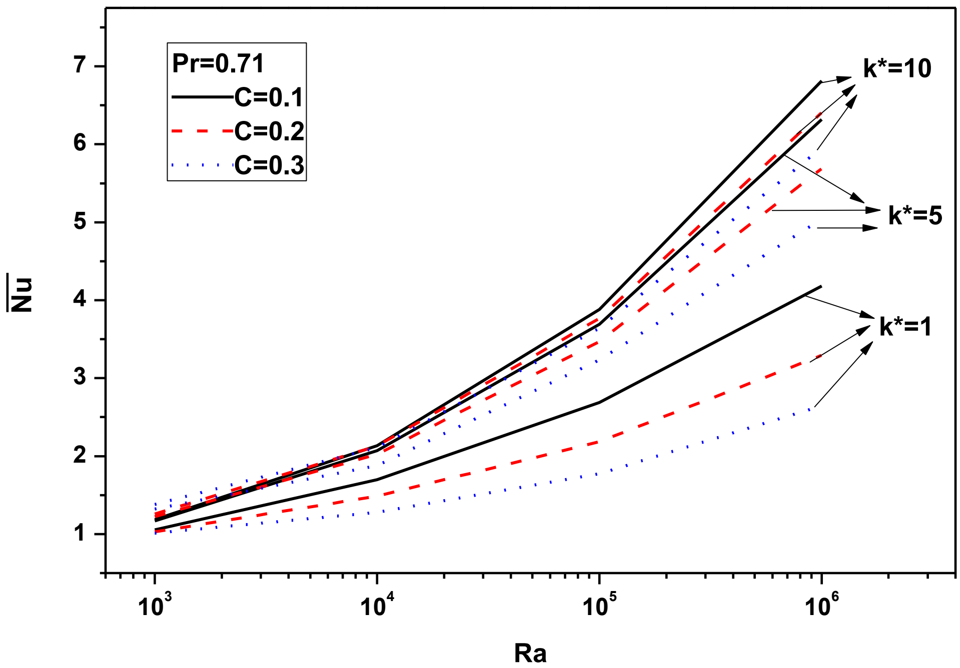

Figure 8. Average Nusselt number as a function of the Rayleigh number for various wall thicknesses (parameter C) and conductivities

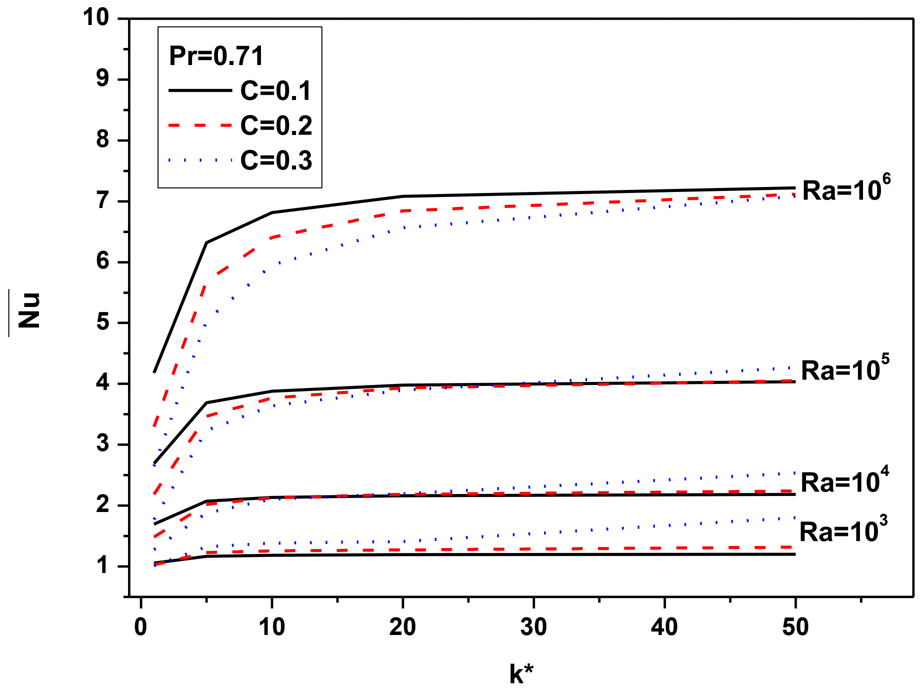

Figure 9. Average Nusselt number as a function of the wall conductivity for various Rayleigh numbers and wall thicknesses (parameter C)

4.3 Effect of the solid size

For the analysis of the effect of the size of the solid block, the effect of the thickness and the length are investigated. Figs 10 and 11 showsthe average Nusselt number as function of the dimensionless wall thickness, from 0 to 0.6 for the range of Rayleigh number (from 10^3 to 10^6). The length of the dimensionless wall (D) chosen for the test is 0.9.

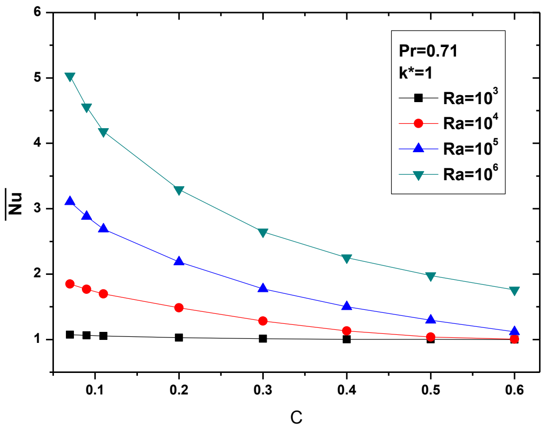

Figure 10. Average Nusselt number for different wall thicknesses and Rayleigh numbers, with k*=1

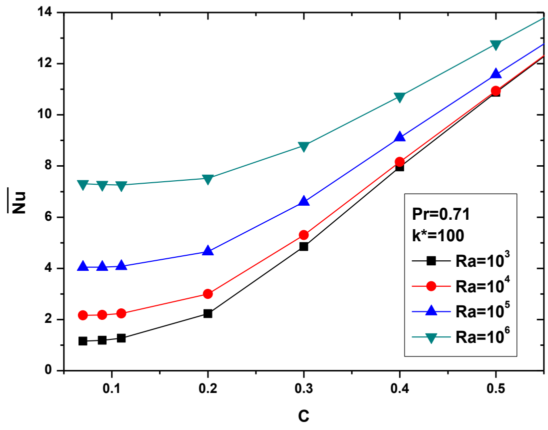

Figure 11. Average Nusselt number for different wall thicknesses and Rayleigh numbers, with k*=100

In the Fig. 10, for k *=1, it can be seen that with increase of the enclosure wall thicknesses, the dimensionless average Nusselt numbers of convection decreases. When the cavity wall thickness exceeds 0.2, the increasing speed of dimensionless average Nusselt numbers of convection decreases. Already for k *=50 (Fig. 11) increase of the enclosure wall thickness, increases the dimensionless average Nusselt number of convection, mainly when it exceeds 0.2. When the cavity wall exceeds certain critical number, the increase of the thickness is invalid for heat transfer.

To evaluate the solid length, we used a wall thickness of 0.1. In Figs. 12 and 13, with increase of the solid length, the dimensionless average Nusselt number of convection decreases linearly, for the different Rayleigh numbers as the solid body becomes larger, the flow interference caused by the solid weakens the fluid flow resulting in a decrease in the Nusselt number as observed in Figs. 12 and 13.

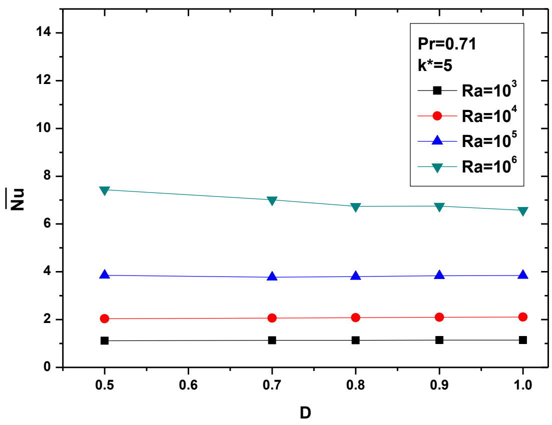

Figure 12. Average Nusselt number for different wall thicknesses and Rayleigh numbers, with k*=5

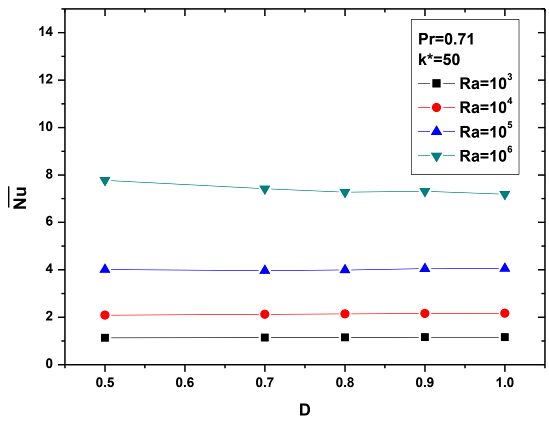

Figure 13. Average Nusselt number for different wall thicknesses and Rayleigh numbers, with k*=50

4.4 Effect of the thermal conductivity of the solid

The average Nusselt number of convection, and the range of k* (from 0.2 to 100) are respectively shown in Figs. 14 to 15, for Rayleigh number of 10^4 and 10^5. In Fig. 15, with increase of the length, the average Nusselt number of convection decreases linearly. With increase of the ratios of the thermal conductivity of cavity wall to the thermal conductivity of air, the change is more clear. In Fig.14, when the ratio of the thermal conductivity of cavity wall to the thermal conductivity of air exceeds the critical number 10 and the critical value 0.2 of thickness, the gradient of average Nusselt number of convection decrease. For k*>10 and C>0.2 the gradient of average Nusselt numbers of convection increases. Due to conduction of enclosure wall, the flow and heat transfer turn to be intense with a certain cavity wall.

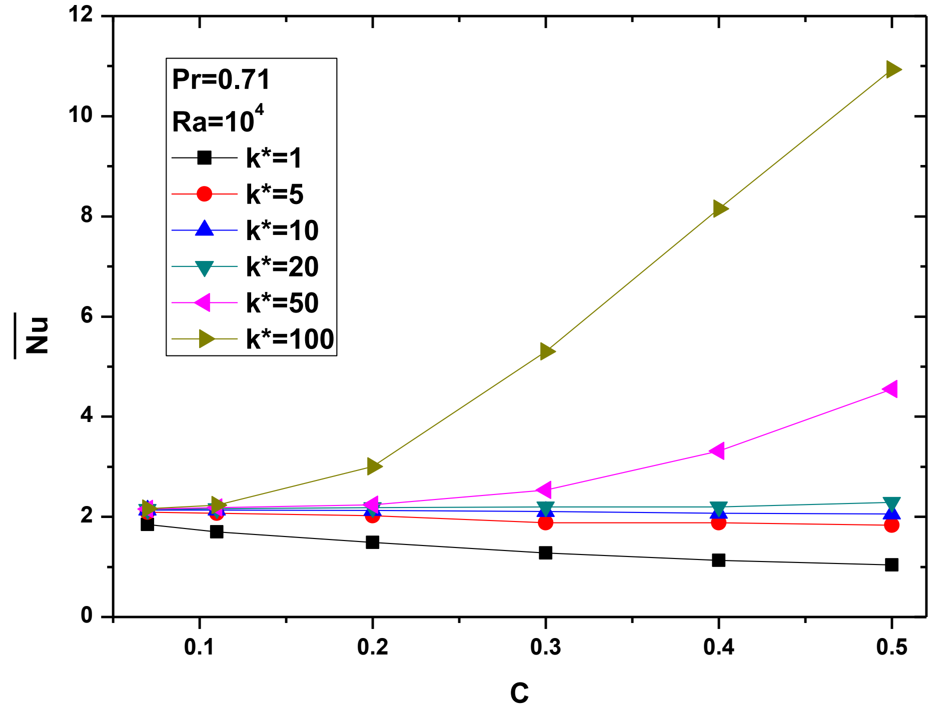

Figure 14. Average Nusselt number for various wall thicknesses (parameter C) and conductivities, with Ra=10^4

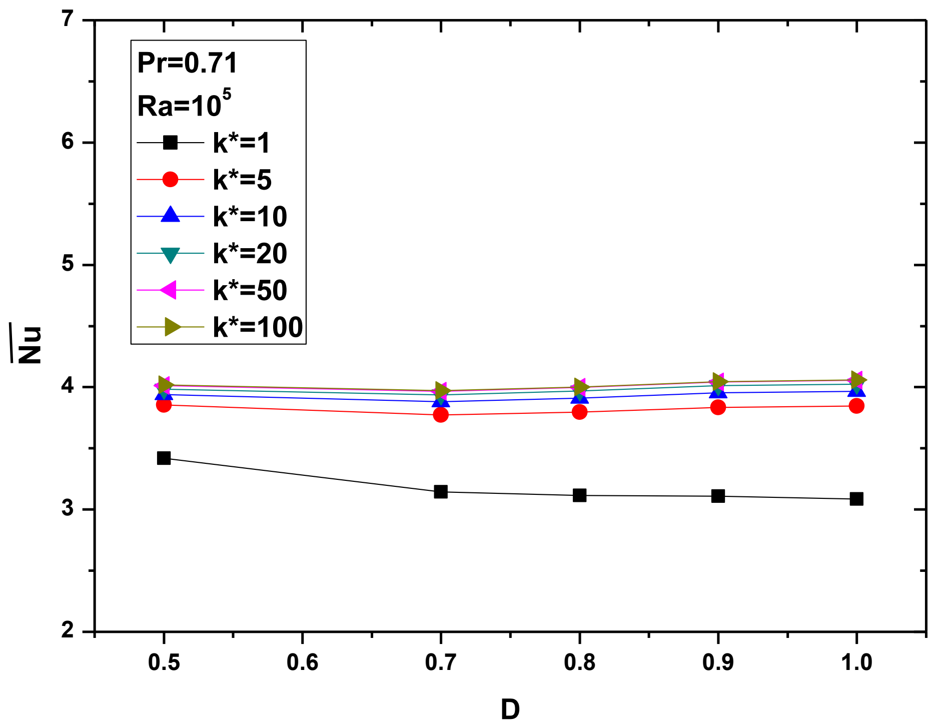

Figure 15. Average Nusselt number for various wall thicknesses (parameter D) and conductivities, with Ra=10^5

5 CONCLUSION

Natural convection in cavity bounded by a solid wall has been studied. Two-dimensional equations of conservation of mass, momentum and energy, with the Boussinesq approximation have been solved using finite volume method. Governing parameters were $10^3 \leq Ra \leq 10^6$; $1 \leq k^* \leq 100$; $0.07 \leq C \leq 0.6$ and $0.5 \leq D \leq 1$. The results showed that heat transfer is an increasing function of the Rayleigh number, wall conductivity ratio, wall thickness and length aspect ratio, it is a decreasing function of the wall thickness para $k<10$, and these trends are amplified at high Rayleigh numbers, at high wall conductivity and small wall thickness. When the cavity wall thickness exceeds a certain critical value, the increase the thickness shows a negligible effect on heat transfer. The temperature distribution changes obviously. When the thermal conductivity of enclosure wall is more than a critical value, the increasing trend of flow and heat transfer may disappear.

This work is very important to investigate the parameters that affect the heat transfer of the conjugate problems in a cavity and can facilitate the development of correlations for numerical simulations of thermal performance of the classic Trombe Wall collector system.

Acknowledgements

The authors wish to thank the CNPQ for the PQ research grant to the second author and for the doctoral scholarship to the first author.

REFERENCES

De Vahl Davis G.,1983. Natural convection of air in a square cavity: a bench mark numerical solution. *Int. J. Numer. Methods Fluids*, vol. 3, pp. 49-64.

Bhave P., Narasimhan A., Rees DAS, 2006. Natural convection heat transfer enhancement using adiabatic block: optimal block size and Prandtl number effect. *Int. J. Heat Mass Transfer*;vol.49, pp. 3807-18.

Frederick, R. L., 1989. "Natural convection in an inclined square enclosure with a partition attached to its cold wall," *Int. J. Heat Mass Transfer,* vol. 32, pp. 87.

Ha MY, Jung MJ, Kim YS, 1999. Numerical study on transient heat transfer and fluid flow of natural convection in an enclosure with a heat-generating conducting body. *Numer. Heat Transfer,* Part A, vol. 35, pp. 415-33.

Ha MY, Kim IK, Yoon HS, Lee S., 2002. Unsteady fluid flow and temperature fields in a horizontal enclosure with an adiabatic body. *Phys. Fluids (1994-Present)*, vol. 14, pp. 3189-202.

Ha MY, Kim IK, Yoon HS, Yoon KS, Lee JR., 2002. Two-dimensional and unsteady natural convection in a horizontal enclosure with a square body. *Numer. Heat Transfer,* Part A, vol. 41, pp. 183-210.

Hernandez-Lopez, I., Xaman, J., Chavez Y., Hernandez-Perez, I., Alvarado-Juarez, R., 2016. Thermal energy storage and losses in a room-Trombe wall system located in Mexico.*Sol.Energy,* vol. 109, pp. 512-524.

House JM, Beckermann C, Smith TF, 1990. Effect of a centered conducting body on natural convection heat transfer in an enclosure. Numer. *Heat Transfer*, Part A, vol.18, pp. 213-22.

Kandaswamy, P., Nithyadevi, N., Chiu-On Ng.,2008.Natural convection in enclosures with partially thermally active side walls containing internal heat sources.*Physics of Fluids*, vol. 20, pp. 097-104.

Kundakci B., Yilmaz Z., 2012. The comparison of Trombe wall systems with single glass, double glass and pv panels. *Energy Build*, vol. 45, pp. 111-8.

Lima, T. P., and Ganzarolli, M. M., 2016. A heat line approach on the analysis of the heat transfer enhancement in a square enclosure with an internal conducting solid body. *Int. Journal of Thermal Sciences*, vol. 105, pp. 45-56.

Liu Y, Wang W, Ma C, Liu J.,2013. A numerical and experimental analysis of the air vent management and heat storage characteristics of a Trombe wall. *Sol Energy*, vol. 91, pp. 1-10.

Mezrhab A, Bouali H, Amaoui H, Bouzidi M., 2006. Computation of combined natural convection and radiation heat-transfer in a cavity having a square body at its center. *Appl. Energy*, vol. 83, pp. 1004-23.

Rabani M, Kalantar V, Dehghan AA, Faghih AK., 2015. Experimental study of the heating performance of a Trombe wall with a new design. *Sol Energy,* vol 118, pp. 359-74.

S. V. Patankar, Numerical Heat Trunsjer and Fluid Flow. Hemisphere, New York (1980).

Yedder, R.B. and Bilgen, E., 1991. Natural convection and conduction in a Trombe wall system, *Int. J. Heat Mass Trans*, vol. 34, pp. 1237-1248.

Zhao FY, Liu D, Tang GF, 2007. Conjugate heat transfer in square enclosures. *Heat Mass Transfer*, vol. 43, pp. 907-22.